



OPEN

## Evaluation of CuS nanorods surface interaction with Cd<sup>2+</sup> ions, Methyl Orange and microbes for clean water management

R. Lakshmi<sup>1</sup>, S. Radjarejesri<sup>2</sup>, Venkatesa Prabhu Sundramurthy<sup>3,4</sup>, Mohamed Abbas<sup>5,6</sup> & Nagaraj Ashok<sup>7</sup>✉

In this study, we report an eco-friendly approach for synthesizing CuS nanorods using aqueous extract of *Syzygium cumini* seeds as a sustainable alternative. The formation of CuS nanorods were confirmed with UV-Vis, SEM and TEM investigations and were found to be around 6–10 nm in length with hexagonal phase. The adsorption of Cd<sup>2+</sup> ions onto CuS nanorods was optimized using Box-Behnken Design. The adsorption capacity of CuS nanorods towards Cd<sup>2+</sup> ions was calculated to be 266.5 mg g<sup>-1</sup>. Based on the error analysis, the Langmuir isotherm and pseudo second order kinetic models were best applicable for the obtained data. Activation energy of 24.73 kJ mol<sup>-1</sup> from Arrhenius equation suggests the physical adsorption of Cd<sup>2+</sup> ions by CuS nanorods. A maximum MO degradation was achieved within 120 min with first order kinetics explaining the degradation process. The CuS nanorods were explored for antimicrobial activity against *E. coli* and *S. aureus* and the zone of inhibitions were high due to the rod shaped CuS nanomaterial with ROS generation being mechanism of activity. These results highlight the ability of the CuS nanorods synthesised in this study in wastewater treatment with microbial activity making it a sustainable material for clean water management.

**Keywords** CuS nanorods, Jamun seeds, Green synthesis, Adsorption, Photocatalysis

Environmental contamination is a major global concern due to their adverse impact on living beings. With globalization and demand for life style changing products, the use of toxic materials and heavy metals have increased and thus leading to environmental pollution. Water pollution is a major concern as the life on earth depends on water for survival. But due to extensive use of water in industries and other non-point sources, water is contaminated to a greater extent and water treatment has become need of the hour<sup>1</sup>. In 2024, 1.2 million deaths were recorded due to water contamination and related diseases which is of concern and UN SDG goal 6 focus on providing clean water and sanitation to all<sup>2</sup>. Researchers are looking towards sustainable solutions to improve water sanitation and provide clean water access to all.

There are a few well established techniques for wastewater treatment that are economical and ecofriendly however adsorption is considered to be one of the efficient and is a pristine technique for the wastewater treatment<sup>3,4</sup>. Especially, the heavy metal and synthetic dyes are effectively removed and recovered for later use<sup>5</sup>. Another advantage of adsorption technique is its ability to photocatalytic degradation of dyes in presence of light source when a suitable adsorbent is chose<sup>6</sup>. Nanomaterials are one class of adsorbents that are superior in adsorption of heavy metal ions, synthetic dyes, emerging contaminants and anions<sup>7,8</sup>. In addition, they also potentially act as prolific catalyst in photo degradation of organic molecules that are considered to be water contaminants<sup>9,10</sup>. To make the use of nanomaterials in wastewater treatment more sustainable, green synthesis of nanomaterials such as noble metals and semiconductor materials are proposed<sup>11</sup>. Various plant and agro-waste

<sup>1</sup>Directorate of Learning and Development, SRM Institute of Science and Technology, Kattankulathur, Tamil Nadu 603203, India. <sup>2</sup>Department of Science, Sona College of Technology, Salem, Tamil Nadu 636005, India. <sup>3</sup>Centre for Natural Products and Functional Foods, Karpagam Academy of Higher Education, Coimbatore, Tamil Nadu 641021, India. <sup>4</sup>Department of Biotechnology, Faculty of Engineering, Karpagam Academy of Higher Education, Coimbatore, Tamil Nadu 641021, India. <sup>5</sup>Central Labs, King Khalid University, PO.Box 960, AlQura'a, Abha, Saudi Arabia. <sup>6</sup>Electrical Engineering Department, College of Engineering, King Khalid University, Abha 61421, Saudi Arabia. <sup>7</sup>Faculty of Mechanical Engineering, Jimma Institute of Technology, Jimma University, Jimma 378, Ethiopia. ✉email: nagaraj.ashok@ju.edu.et

extracts were explored for the green synthesis of semiconductor-based nanomaterials and effectively used in the adsorption of heavy metal ions and photodegradation of synthetic dyes<sup>12,13</sup>. Plant and fruit waste contains numerous biomolecules that can effectively reduce, cap and stabilize the nanomaterials formations<sup>14</sup>.

In a study, neem leaf extracts were utilized for the synthesis of ZnO, CuO and NiO nanomaterials and used in the photodegradation of methylene blue dye under sunlight<sup>15</sup>. The synthesized nanomaterials exhibited excellent photocatalytic activity under sunlight with CuO being more efficient comparatively. ZnO nanoparticles were synthesized using *Nauclea latifolia* fruit extract with a particle size around 15 nm and used in the adsorption performance towards Cango red<sup>16</sup>. The ZnO nanoparticles exhibited 99.9% removal efficiency towards Cango red within 60 min of time. Broccoli extracts were explored for the synthesis of ZnS nanoparticles with 2.57 nm in size having zinc blende phase<sup>17</sup>. The synthesized ZnS nanoparticles exhibited photocatalytic ability towards methylene blue cationic dye. Watermelon rind extracts were employed in facile synthesis of CdS nanoparticles with a size aspect of 10 nm and used in the adsorption of methylene blue and crystal violet dyes<sup>18</sup>. Spherical shaped CuO nanoparticles were successfully synthesized by *Inula* genus plant extract with a size of 20 nm and used in the adsorption of Pb<sup>2+</sup> ions<sup>19</sup>. The CuO nanoparticles exhibited a loading capacity of 124.7 mg g<sup>-1</sup> under optimized conditions using RSM. A green alga was explored in the synthesis of CuS nanoparticles with a size aspect of 9–23 nm and used in the photodegradation of methylene blue dye<sup>20</sup>. CuS nanoparticles using Xanthum gum was explored as an efficient photocatalyst for the degradation of methylene blue, cango red, rhodamine B and eosin y dyes<sup>21</sup>. The nanoparticles were found to be around 8–20 nm in size and exhibited activity under various light sources.

Cadmium is one among the heavy metal ions that exhibit toxicity to human and wildlife and considered to be carcinogenic. Their presence in water leads to bioaccumulation in food chain and lead to various ill effects at lower concentrations. Adsorption is one of the efficient process for the removal of Cd<sup>2+</sup> ions by nanoparticles and various nanomaterials are explored for the removal of Cd<sup>2+</sup> ions from aqueous solution<sup>22</sup>. Methyl Orange (MO) is a water-soluble recalcitrant dye that is hard to degrade and pose health risk when they are present in water streams<sup>23</sup>. It is commonly used as pH indicator in labs and easily comes into the water streams<sup>24</sup>. Considering their potential impact and ability to biotransformation to benzidine it is essential to eliminate or decolorize from water streams. Photocatalysis is one of the promising techniques for the elimination of MO from wastewaters and nanomaterials are pioneers in the degradation process with enhanced efficiencies<sup>25</sup>. Semiconductor based nanomaterials play a significant role in the decolorization process as reported in the literature<sup>26</sup>. Microbial contamination is one of the serious threats to human because they contaminate the food and water leading to unhealthy conditions<sup>27</sup>. *E. coli* (Gram-negative) and *S. aureus* (Gram-positive) are common microorganisms that contaminate various settings and require careful attention. Antimicrobial agents based on nanomaterials formulations play a vital role in killing the microbes effectively<sup>28</sup>. Several nanomaterials synthesized via green route have exhibited enhanced activity towards potential microbes and CuS nanoparticles have proven to be effective<sup>29,30</sup>.

While CuS nanoparticles have been explored for heavy metal adsorption, dye photodegradation, and antimicrobial activity, most studies are limited to spherical morphologies via green synthesis, with a focus on single applications. Shape-controlled synthesis, particularly nanorods, remains unexplored despite their potential for enhanced performance due to higher aspect ratios and reactive facets. Furthermore, a systematic approach combining environmental and biomedical applications with statistical optimization is lacking. In this study, we report the first green synthesis of CuS nanorods using *Syzygium cumini* seeds, achieving precise shape control. The dual functionality of these nanorods efficient heavy metal adsorption and potent antimicrobial activity is demonstrated, with statistical optimization ensuring reproducibility. This work bridges the gap between nanomaterials design and multifunctional real-world applications. All the experiments were performed in triplicates and their mean values are reported.

## Materials and methods

### Materials

Cu(NO<sub>3</sub>)<sub>2</sub> and Na<sub>2</sub>S were purchased from sigma Aldrich chemicals with 99.9% purity. HCl and NaOH of AR grade were obtained from Merck chemicals and made to appropriate molar solutions using double distilled water. Methyl Orange was procured from Nice chemicals and used after dilution to lower concentrations. Double distilled water was used for all dilutions and experimental solutions.

### Preparation of aqueous extract of seeds

*Syzygium cumini* is a flowering plant family of *Myrtaceae* and are commonly known as Indian Jamun that are widely cultivated in Southeast Asia. The seeds of the jamun fruit are reported to have several medicinal benefits and commonly used in the Ayurveda medicines<sup>31</sup>. The jamun seeds are well documented and were collected from a local fruit market and thoroughly washed with running tap water to remove impurities. The cleaned seeds were dried under sunlight for seven days. After drying, the seed shells were removed, and the seeds were ground into a fine powder using a conventional grinder. The resulting powder was stored in an airtight container for later use in preparing an aqueous extract. To prepare the aqueous extract, 2 g of jamun seed powder was mixed with 100 mL of deionized water and heated at 65 °C with continuous stirring for 120 min. The yellowish solution obtained was filtered using Whatman filter paper to remove any solid residues. This freshly prepared aqueous extract was then used as a reducing and stabilizing agent for synthesizing CuS nanorods.

### Synthesis of CuS nanorods

To synthesize CuS nanoparticles, a 0.1 M solution of Na<sub>2</sub>S was prepared. Then, 25 mL of this solution was combined with 25 mL of the jamun seed aqueous extract and stirred on a magnetic stirrer to achieve a homogeneous mixture and pH was adjusted to 6 with 0.01 M HCl solution. Subsequently, 25 mL of 0.1 M Cu(NO<sub>3</sub>)<sub>2</sub> solution

was added dropwise to the mixture with continuous stirring. The addition of the  $\text{Cu}(\text{NO}_3)_2$  solution led to the appearance of a blackish green precipitate, indicating the formation of the  $\text{CuS}$  compound. After the addition was complete, the reaction mixture was stirred continuously for another 2 h at  $80^\circ\text{C}$  on a magnetic stirrer to facilitate capping and size/shape control of the  $\text{CuS}$  nanoparticles by the biomolecules. The resulting mixture was then centrifuged at 10,000 rpm to separate the  $\text{CuS}$  nanoparticles, which were subsequently dried in an oven. The dried nanoparticles were stored in an airtight container for further characterization (Scheme 1).

### Characterization techniques

The  $\text{CuS}$  nanorods were characterized using various analytical techniques. The absorption bands were analyzed using a Shimadzu UV-Visible Spectrophotometer (UV3600 Plus). Surface functional groups were identified with FTIR spectroscopy (Shimadzu IRTracer-100) in ATR mode, covering a range of  $4000\text{--}400\text{ cm}^{-1}$ . The crystallographic structure was examined through powder X-ray diffraction (PANalytical, Netherlands), while the surface morphology was investigated using a Scanning Electron Microscope (Supra 55, Carl Zeiss, Germany). The size and shape of the nanoparticles were further studied with Transmission Electron Microscopy (G2-20 Twin FEI Tecnai) operated at 200 kV. Additionally, the residual concentration of  $\text{Cd}^{2+}$  ions was determined using an Atomic Absorption Spectrophotometer (Varian AA240), with the hollow cathode lamp set at 228.8 nm, utilizing acetylene as the fuel and air as the oxidant.

### Batch adsorption experiments

Batch experiments were performed for 50 ml of test solutions at 100 rpm according to the BBD matrix to evaluate the  $\text{CuS}$  nanorods adsorption ability. The test solutions post adsorption was centrifuged and the supernatant solution was subjected to atomic absorption spectrophotometer to determine the residual concentrations of the  $\text{Cd}^{2+}$  ions. The removal efficiency and loading capacities were calculated with the following Eq.

$$\% \text{ } \text{Cd}^{2+} \text{ ions removal} = \left( \frac{C_O - C_1}{C_O} \right) \times 100 \quad (1)$$

$$\text{CuS nanorods loading capacity (mg/L)} = \left( \frac{C_O - C_1}{M} \right) V \quad (2)$$

Where  $C_O$  is the initial concentration of the  $\text{Cd}^{2+}$  ions and  $C_1$  is the residual concentration of the  $\text{Cd}^{2+}$  ions in the solution.  $V$  is the volume of the solution and  $M$  is the mass of the  $\text{CuS}$  nanorods.

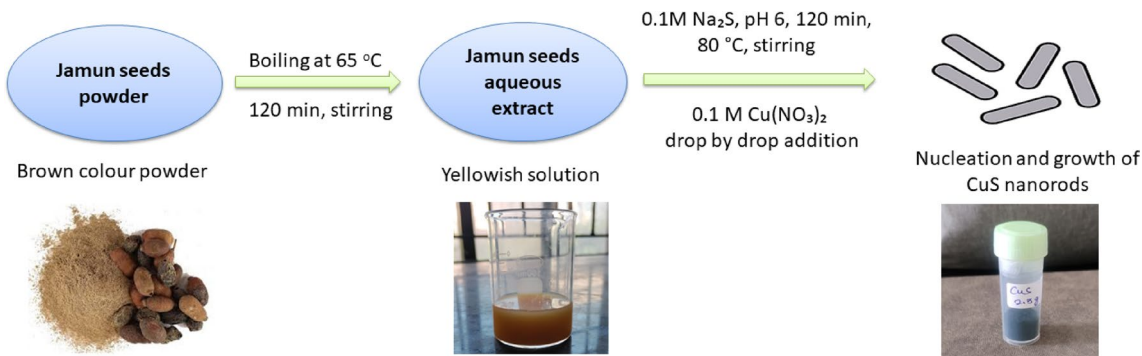
### RSM

Box Behnken Design (BBD) of Response Surface Methodology (RSM) was employed to optimize the independent variables that crucially govern the adsorption of adsorbate and adsorbent. To design the experiments, variables such as pH, contact time and initial concentrations were selected with three levels for each factor ( $-1, 0, +1$ ) with a total of 17 experimental runs (Table 1). The BBD matrix was developed using Design expert software.

### Photocatalysis

The catalytic performance of the  $\text{CuS}$  nanorods produced by jamun seeds to decolourize the Methyl Orange (MO) dye was investigated. Experiments for photocatalytic activity were carried out by addition of 0.1 g of  $\text{CuS}$  nanorods to  $100 \text{ mg L}^{-1}$  of 100 ml of MO solution with constant stirring. The test solution was placed in a photo reactor equipped with UV source to deliver the desired light for the photocatalytic activity and sample aliquots of 5 mL were drawn at regular time intervals between 10 and 150 min. The residual concentrations of MO was tested with UV-Visible spectrophotometer at 465 nm and determined with the following equation:

$$\% \text{ MO decolourized} = \frac{MO_0 - MO_t}{MO_0} \times 100 \quad (3)$$



**Scheme 1.** Schematic diagram of synthesis of  $\text{CuS}$  nanorods by jamun seeds aqueous extract.

Variables	Symbol	Levels		
		-1	0	+1
pH	A	4	6	8
Contact time (min)	B	30	65	150
Initial concentration (mg L <sup>-1</sup> )	C	50	175	300

**Table 1.** Independent variables, their levels and symbols used in this study for Cd<sup>2+</sup> ion adsorption by CuS nanorods.

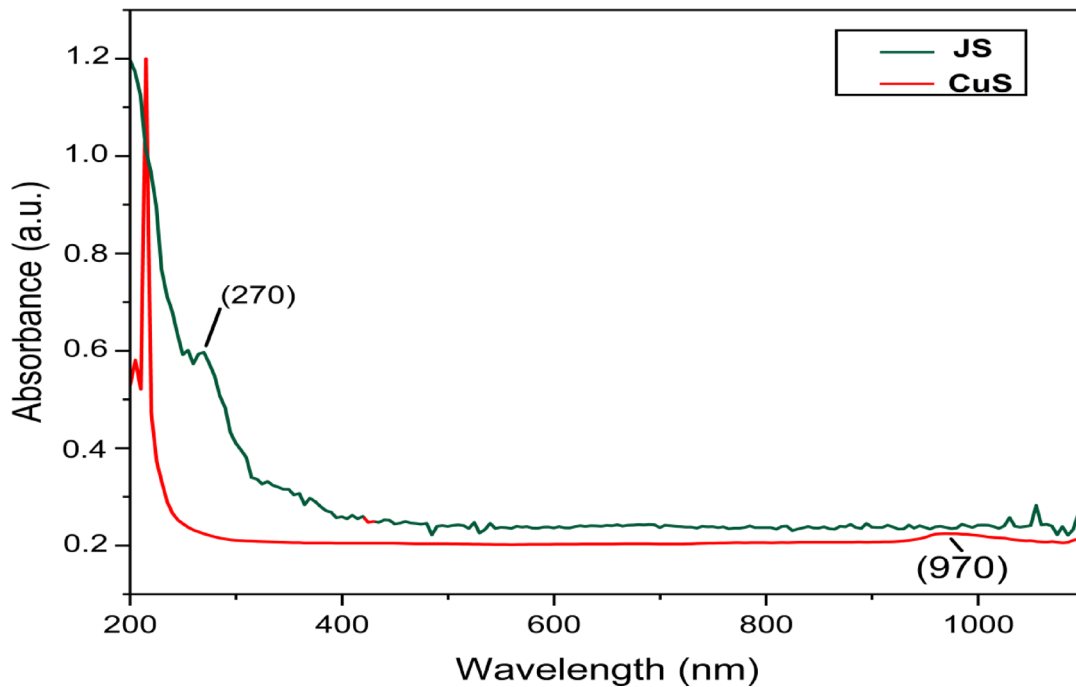


**Fig. 1.** UV-Visible plot of CuS nanorods and Jamun seeds aqueous extract.

Where  $MO_0$  is initial MO concentration and  $MO_t$  is final concentration.

#### Antimicrobial activity

The antibacterial activity of CuS nanorods was assessed via the agar well diffusion technique on Mueller-Hinton Agar (MHA). Under sterile conditions, MHA was poured into Petri dishes and allowed to solidify at room temperature for one hour. Overnight cultures of *E. coli* (Gram-negative) and *S. aureus* (Gram-positive) were adjusted to  $\sim 10^8$  CFU/mL (equivalent to the 0.5 McFarland standard) and uniformly swabbed onto the MHA surface. Wells (7–8 mm in diameter) were punched into the agar using a sterile cork borer. CuS nanorod suspensions, prepared in sterile distilled water, were added (50  $\mu$ L per well). The plates were left at room temperature for 30 min to permit nanoparticle diffusion before incubation at 37 °C for 24 h to observe bacterial growth and nanoparticle interaction. Following incubation, the inhibition zones (ZOI) surrounding the wells were measured with a calibrated ruler to determine antibacterial efficacy. All tests were conducted in triplicate for reproducibility and statistical validity.

#### Results and discussion

##### UV-Vis

The absorption spectrum of CuS nanorods and seed extract are presented in Fig. 1 and interestingly there was only one band observed in the range of 300–1200 nm with a peak maximum at 970 nm in the NIR region however the extract exhibited peaks only in 200–300 nm range due to presence of biomolecules. A peak in the NIR region exhibited by the CuS nanorods is due to the ability of the nanorods to observe energy in the visible and near infrared region which confirms the covellite CuS<sup>32,33</sup>. Further the band gap of the CuS nanorods were calculated from Tauc plot and determined to be 1.9 eV. The observation is consistent with other reports on covellite CuS nanorods produced from wet chemical methods<sup>34</sup>.

### FTIR

The FTIR spectra of CuS nanorods and seed extract provided information on the functional groups present on the surface of the nanorods and the functional groups of seed extract (Fig. 2). The seed extract indicated various functional groups that hint the capping and stabilization of nanorods. The FTIR of CuS nanorods present various peaks corresponding to various functional groups that were observed in the seed extract. A sharp peak at  $3550\text{ cm}^{-1}$  corresponds to the  $-\text{O}-\text{H}$  free hydroxyl group of phenols and a peak at  $3365\text{ cm}^{-1}$  is due to hydrogen bonded hydroxyl group stretching<sup>35</sup>. A peak at  $3298\text{ cm}^{-1}$  is due to the stretching of  $\text{N}-\text{H}$  groups of amine and peak at  $2970\text{ cm}^{-1}$  is due to the  $-\text{CH}$  stretching vibrations. Peaks at  $1629$  and  $1578\text{ cm}^{-1}$  corresponds to the  $-\text{C}=\text{O}$  stretching of carboxyl group and  $-\text{C}=\text{C}$  of aromatic ring of phenolic groups. Peaks at  $1074$  and  $1030\text{ cm}^{-1}$  corresponds to the stretching of  $-\text{C}-\text{O}$  group of alcohol and bands at  $953$  and  $844\text{ cm}^{-1}$  are bending vibrations of  $-\text{C}-\text{H}$  groups from alkenes and aromatic compounds. A small and sharp band at  $468\text{ cm}^{-1}$  corresponds to the Cu-S stretching vibrations confirming the formation of CuS compound<sup>36</sup>. Various bands seen in the FTIR spectra suggest that the biomolecules from jamun seed extract have successfully capped and stabilized the formation of CuS nanorods. Similar results were reported for the green synthesis of CuO nanoparticles<sup>37</sup>.

### XRD

The CuS nanorods were subjected to XRD analysis to understand the diffraction patterns and the results are depicted in Fig. 3. The pattern depicts characteristic peaks at various  $2\theta$  values suggesting the crystalline nature of the CuS nanorods. The  $2\theta$  values of  $22.3, 27.2, 29.4, 31.8, 48.1, 52.8$  and  $59.1$  corresponds to hexagonal phase of  $004, 101, 102, 103, 110, 114$ , and  $116$  planes<sup>20</sup>. The planes obtained in this study references to JCPDS card no. 001-1281. The crystallite size of the CuS nanorods were calculated using Debye Scherrer equation and found to be around  $9.5\text{ nm}$ . This is good agreement with CuS nanoparticles synthesized by green route<sup>38</sup>.

### SEM

The surface morphology of the CuS nanorods were visualized with SEM analysis and the results are presented in Fig. 4a, b. The images reveal needle like structures depicting the smaller nanorods and found to be agglomerated due to close packing of the samples. Furthermore, the formation of nanorods indicates the role of a particular biomolecule from the seed extract assisting as a template for the nanorods formation<sup>39</sup>. The irregular shapes observed in the image are due to the variations in nucleation and growth kinetics under non-equilibrium conditions. The EDX pattern obtained for the CuS nanorods confirms the purity of nanorods formation with Cu and S peaks and absence of other elements (Fig. 4c).

### TEM

The CuS nanostructures synthesised with jamun seed extracts were subjected to TEM analysis to confirm the formation of nanorods visualized in SEM analysis. The images revealed the successful formation of CuS nanorods in addition to irregular shaped particles as observed in SEM images. The nanorods were around  $6\text{--}10\text{ nm}$  in

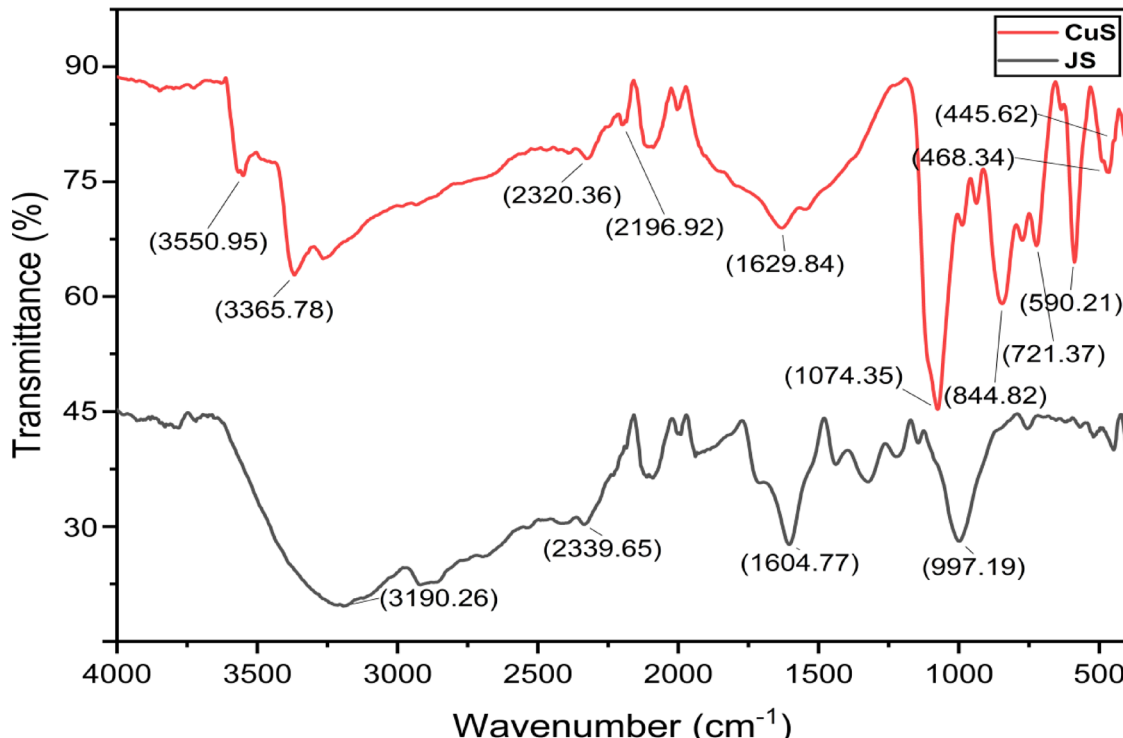


**Fig. 2.** FTIR spectra of CuS nanorods and Jamun seeds aqueous extract.

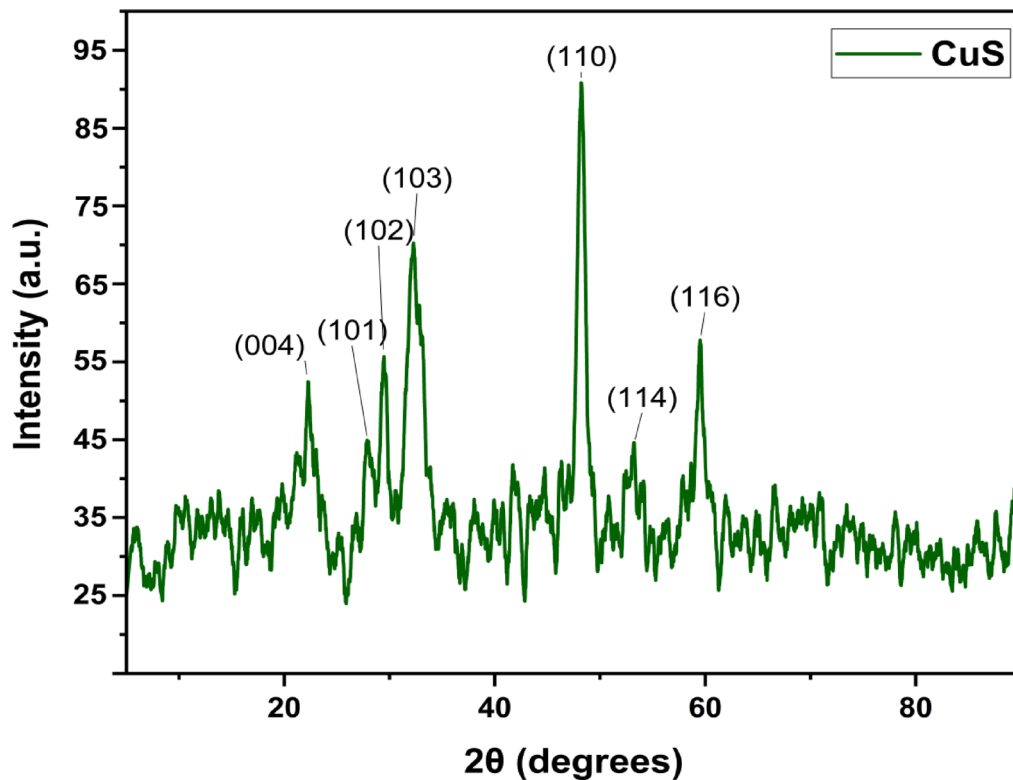


**Fig. 3.** XRD pattern of CuS nanorods synthesised using jamun seeds aqueous extract.

length with a width of around 4 nm (Fig. 5). The nanorods were observed to be stacked up on each other due to complex biomolecules present in the jamun seed extract that capped the CuS nanostructures.

#### Box Behnken design

BBD is one of the powerful methods to optimise the independent variables and the results of the experiments in the form of % removal are represented in Table 2. It can be noticed that the experimental and predicted % removal are in good agreement for all the runs suggesting the suitability of the design. Further the uniform distribution of predicted and experimental values along the straight line validates the model significance (Fig. 6a). The ANOVA of the experimental results are summarized in Table 3. F-value and p-value obtained for the removal of Cd<sup>2+</sup> ions by CuS nanorods are found to be 740.13 and < 0.0001 which defines the significance of the model. The lack of fit value was noted to be 4.71 with a p-value of < 0.1302 which was found to be insignificant suggesting the suitability of the model for predicting the experimental results. The correlation coefficients predicted and adjusted are very close to the obtained R<sup>2</sup> values highlighting the importance of the developed design<sup>40</sup>. The adequate precision was calculated to be 72.42 which is very high suggesting the ability of the model to explain the adequate signal for accuracy and the Box-cox plot lambda was determined to be 1 suggesting that no transformations are required for the model Fig. 6b. The standard deviation for the statistical analysis of the data was noted to be 1.37 which further validates the experimental fit to the model. The experimental quadratic polynomial equation for the removal of Cd<sup>2+</sup> ions by CuS nanorods is presented in Eq. 4.

$$\begin{aligned} \text{Removal} = & 83.14 + 2.70A + 13.41B - 19.54C + 6.72AB - 0.17AC \\ & + 1.35BC - 37.45A^2 - 15.07B^2 - 10.12C^2 \end{aligned} \quad (4)$$

The 3D surface plots obtained for the interaction of the independent variables selected in this study are represented in Fig. 7a–c. The interaction between pH and contact time shows the optimal values for the maximum removal of Cd<sup>2+</sup> ions by CuS nanorods (Fig. 7a). The removal efficiency increases with increase in pH and found to be maximum around pH 6 and later found to be decrease with rise in pH value. The maximum efficiency observed at pH 6 can be further explained with pH<sub>pzc</sub> value of the CuS nanorods which was experimentally determined to be at pH 3.7. Accordingly, if the pH value is below pH<sub>pzc</sub> then the surface will be positive that will repel the cation at the surface. If the pH is above pH<sub>pzc</sub>, then the surface of the CuS nanorods will be negative and it will attract the positively charged Cd<sup>2+</sup> ions to its surface. However, at lower pH the H<sup>+</sup> ions also compete for the surface sites and hence the efficiency is minimal but with raises in pH the H<sup>+</sup> ions concentration decreases and thus Cd<sup>2+</sup> ions adsorption increases. In addition to the pH, contact time also influences the efficiency and higher contact time results in higher removal of Cd<sup>2+</sup> ions. Higher times provide sufficient interaction time for the Cd<sup>2+</sup> ions onto the surface of the CuS nanorods leading to greater adsorption and removal.

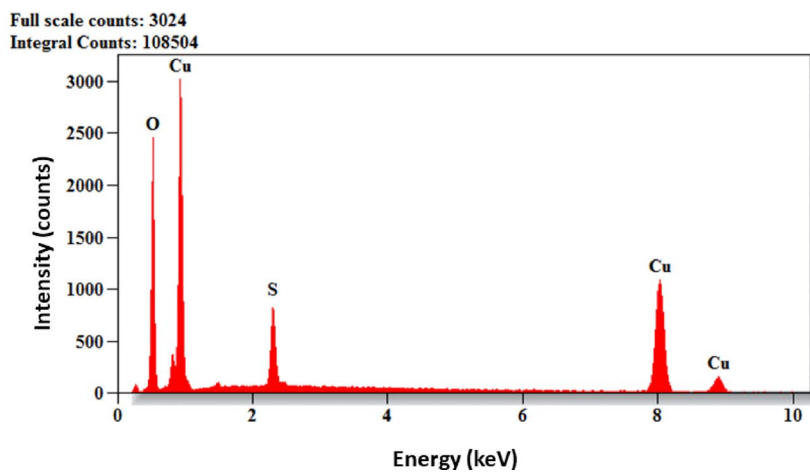
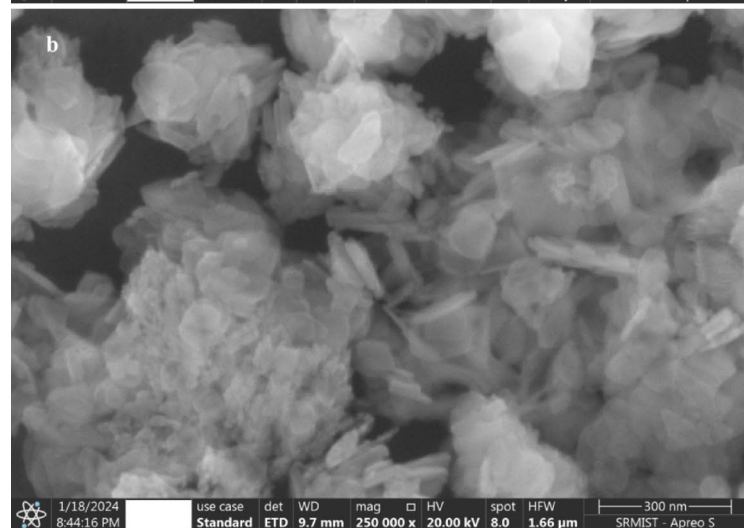
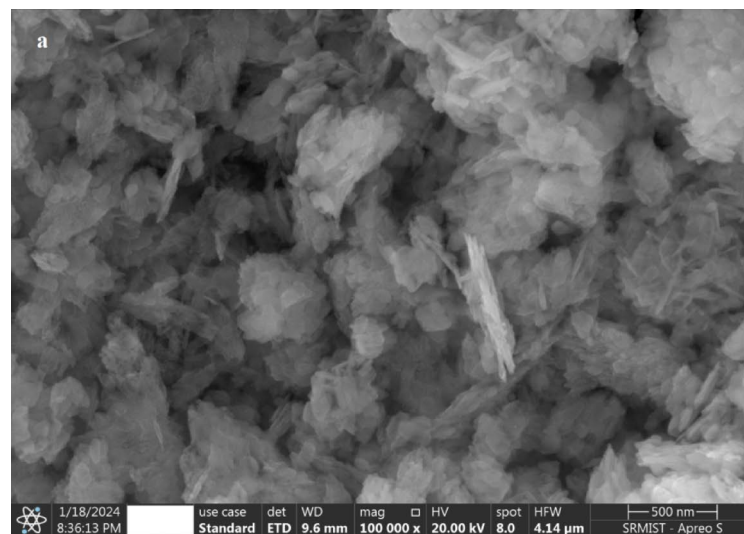


**Fig. 4.** (a,b) SEM images and (c) EDX pattern of CuS nanorods synthesised using jamun seeds aqueous extract.

The interaction of pH with initial concentration of  $\text{Cd}^{2+}$  ions and their influence on removal by CuS nanorods is depicted in Fig. 7b. It can be noticed that maximum adsorption is noticed at pH 6 irrespective of the initial concentrations. However with rise in  $\text{Cd}^{2+}$  ions concentrations, the removal efficiency declines even though the pH remains optimal and this could be attributed to the disappearance of active sites on the surface of CuS

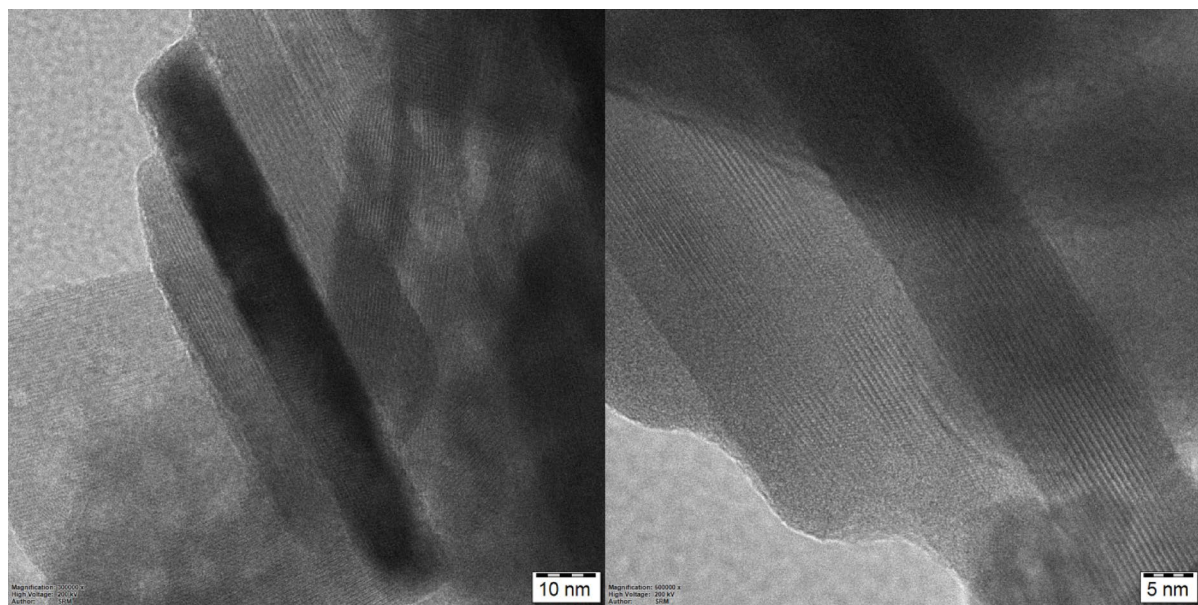


**Fig. 5.** TEM images of CuS nanorods synthesised using jamun seeds aqueous extract.

Std	Run	A: pH	B: Contact time min	C: Initial concentration mg L <sup>-1</sup>	Removal %	
					Experimental	Predicted
16	1	6	65	175	83.2	83.14
17	2	6	65	175	83.4	83.14
11	3	6	10	300	22.6	23.65
7	4	4	65	300	15.3	13.51
2	5	8	10	175	14.3	13.19
6	6	8	65	50	56.2	57.99
8	7	8	65	300	18.5	18.56
4	8	8	120	175	54.2	53.46
14	9	6	65	175	83.2	83.14
9	10	6	10	50	66.1	65.42
3	11	4	120	175	33.5	34.61
10	12	6	120	50	90.6	89.55
13	13	6	65	175	82.9	83.14
15	14	6	65	175	83.0	83.14
12	15	6	120	300	52.5	53.17
5	16	4	65	50	52.3	52.24
1	17	4	10	175	20.5	21.24

**Table 2.** Box Behnken design matrix for the removal of Cd<sup>2+</sup> ions by CuS nanorods.

nanorods due to binding of Cd<sup>2+</sup> ions. Similarly, for the interaction of contact time and initial concentration, the removal efficiency is noted to be maximum at higher contact times and lower Cd<sup>2+</sup> ions concentration (Fig. 7c). Higher concentrations with longer contact times yields lower removal percentage due to saturation of active sites on CuS nanorods. Thus, the surface plots depict clear picture of optimal conditions and the interactions of the independent variables for the maximum removal of Cd<sup>2+</sup> ions by CuS nanorods.

### Adsorption investigations

The equilibrium data at various concentrations were analysed with four isotherm models and the respective parameters constants and correlation coefficients are summarised in Table 4. The non-linear equation plots of four isotherm models fitting are represented in Fig. 8. It is noticed that the Langmuir isotherm found to have better correlation coefficients compared to other three isotherms. However, the correlation coefficients of other three isotherms are also close to one suggesting their applicability. It is crucial to investigate the other parameters of the isotherms to understand the mechanism of the Cd<sup>2+</sup> ions removal by CuS nanorods. The  $q_m$  calculated from the Langmuir isotherm was found to be 275.4 mg g<sup>-1</sup> and this is in close agreement to the experimental

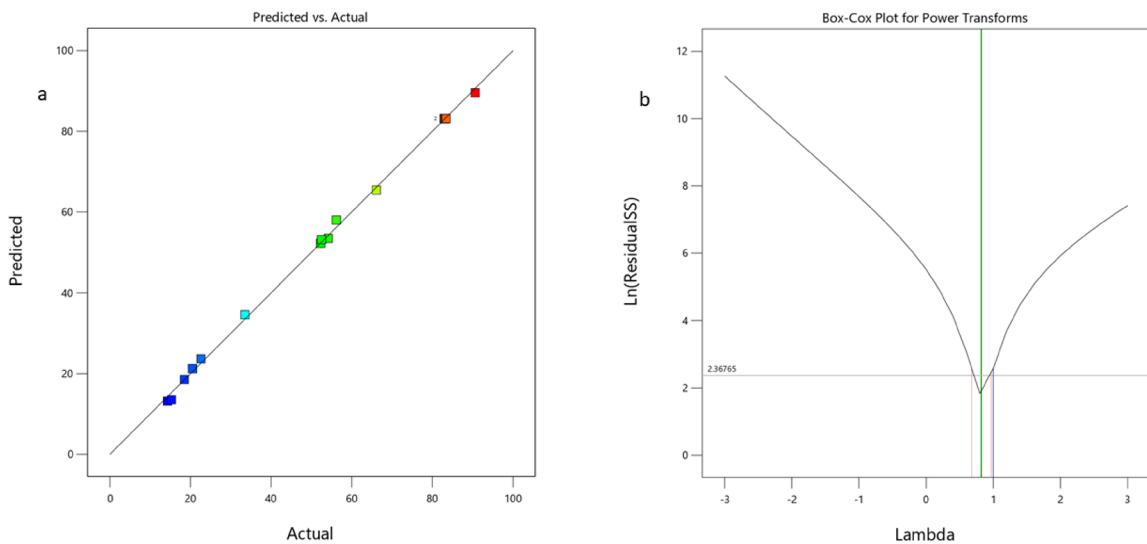


**Fig. 6.** Predicted and actual plot and Box-Cox plot obtained for the removal of  $\text{Cd}^{2+}$  ions by CuS nanorods.

Source	Sum of squares	Degrees of freedom	Mean square	F-value	p-value
Model	12589.19	9	1398.80	740.13	<0.0001
A-pH	58.32	1	58.32	30.86	0.0009
B-Contact time	1439.16	1	1439.16	761.49	<0.0001
C-Initial concentration	3053.71	1	3053.71	1615.78	<0.0001
AB	180.90	1	180.90	95.72	<0.0001
AC	0.1225	1	0.1225	0.0648	0.8064
BC	7.29	1	7.29	3.86	0.0903
$A^2$	5903.70	1	5903.70	3123.77	<0.0001
$B^2$	956.23	1	956.23	505.96	<0.0001
$C^2$	431.22	1	431.22	228.17	<0.0001
Residual	13.23	7	1.89		
Lack of fit	13.08	3	4.36	4.71	0.1302
Pure error	0.1520	4	0.0380		
Cor total	12602.42	16			
$R^2$	Adjusted $R^2$	Predicted $R^2$	Adequate precision	Std deviation	
0.999	0.997	0.983	72.42	1.37	

**Table 3.** ANOVA of  $\text{Cd}^{2+}$  ions removal by CuS nanorods.

values which is calculated to be  $266.5 \text{ mg g}^{-1}$ . The  $K_L$  value of  $0.0296 \text{ L mg}^{-1}$  indicates strong affinity of  $\text{Cd}^{2+}$  ions towards CuS nanorods and primarily can be attributed to the strong coordination to sulphur sites by the  $\text{Cd}^{2+}$  ions. The  $K_F$  and  $n$  of Freundlich constant was calculated to be 61.25 and 2.89 and  $n$  value  $> 1$  suggests the favourable adsorption of  $\text{Cd}^{2+}$  ions onto CuS nanorods<sup>41</sup>. The  $q_s$  value which indicates the theoretical saturation capacity of CuS nanorods are determined to be  $263.18 \text{ mg g}^{-1}$  which is in good agreement to the experimental value. The mean free energy was calculated to be  $15.41 \text{ KJ mol}^{-1}$  suggesting ion-exchange (physisorption) as dominating mechanism for the  $\text{Cd}^{2+}$  ions removal by CuS nanorods<sup>42,43</sup>. The  $A_T$  value was calculated to be  $0.186 \text{ L mg}^{-1}$  and the low value indicates the moderate  $\text{Cd}^{2+}$  ions repulsion on CuS nanorods surface at high surface coverage. The  $b_T$  value of  $125.6 \text{ J mol}^{-1}$  suggests the physical adsorption of  $\text{Cd}^{2+}$  ions onto CuS nanorods. The investigation of each isotherm parameter provided valuable information on the  $\text{Cd}^{2+}$  ions by CuS nanorods however to identify the best isotherm model that is statistically significant, additional analysis on error metrics were performed and the results are summarized in Table 5. The results suggest that the Langmuir isotherm has the lowest errors with highest  $R^2$  confirming the best of the model to the  $\text{Cd}^{2+}$  ions removal by CuS nanorods compared to other three isotherm models. Temkin has the highest errors followed by the Freundlich isotherm and D-R isotherms.

### Kinetics of adsorption

The kinetic data obtained for the  $\text{Cd}^{2+}$  ions removal by CuS nanorods were analysed with various kinetic models and the responses are summarised in Table 6 and plots are represented in Fig. 9. The kinetic data reveals

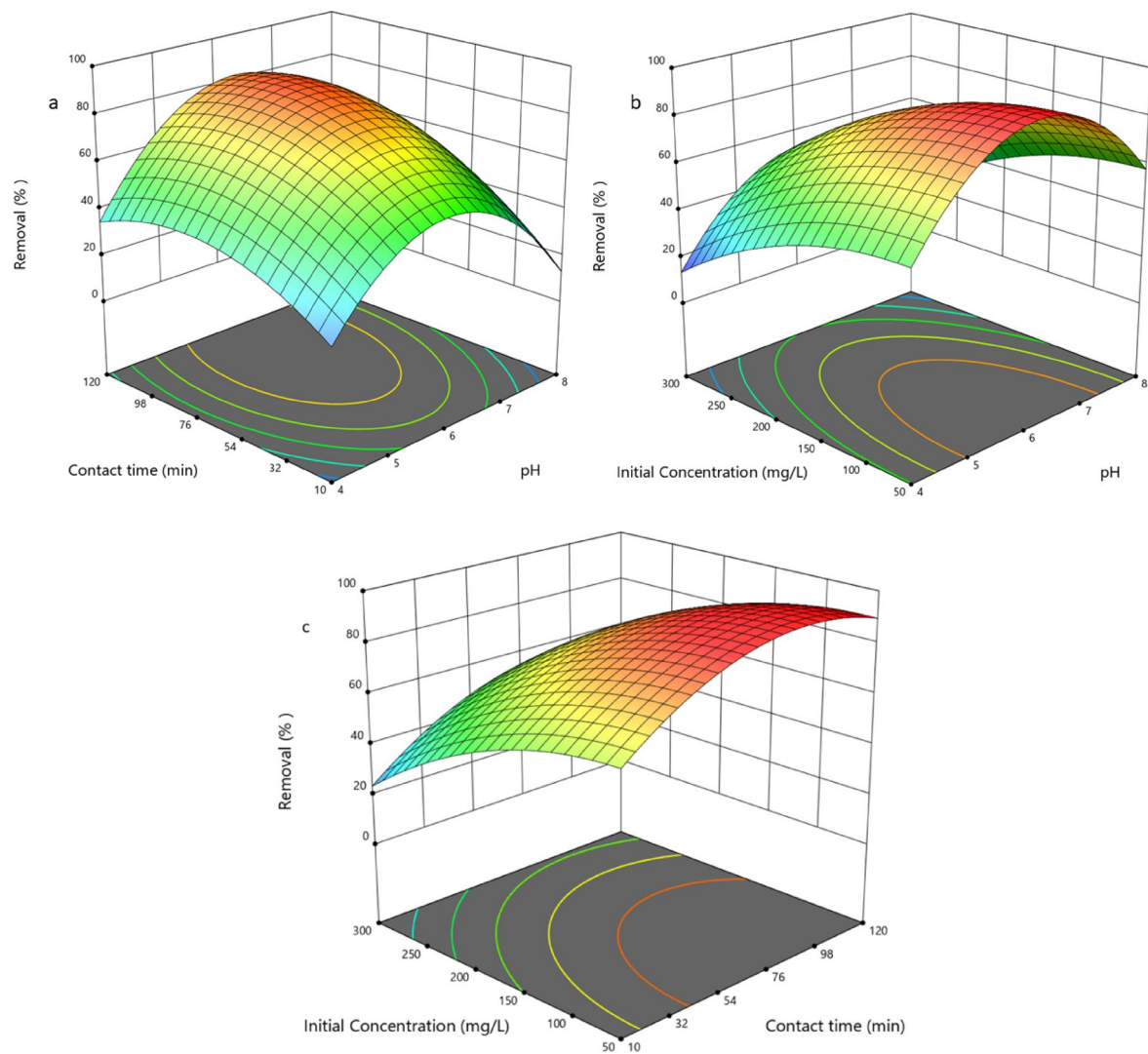


**Fig. 7. (a–c)** 3D Surface plots of  $\text{Cd}^{2+}$  ions removal by CuS nanorods synthesised by jamun seeds aqueous extract.

Isotherm	Parameters	Value
Langmuir $q_e = \frac{Q_m K_L C_e}{1 + K_L C_e}$	$Q_m$ ( $\text{mg g}^{-1}$ )	275.4
	$K_L$ ( $\text{L}^{-1} \text{mg}$ )	0.029
	$R^2$	0.991
Freundlich $q_e = K_F C_e^{1/n}$	$K_F$ ( $\text{mg g}^{-1} \text{L mg}^{-1}$ )	61.25
	$n$	2.89
	$R^2$	0.963
D-R $q_e = q_s \exp(-K_{DR} [RT \ln(1 + \frac{1}{C_e})]^2)$	$Q_s$ ( $\text{mg g}^{-1}$ )	263.18
	$K_{DR}$ ( $\text{mol}^2 \text{kJ}^2$ )	0.0021
	$E$ ( $\text{kJ mol}^{-1}$ )	15.41
	$R^2$	0.978
	$A_T$ ( $\text{L mg}^{-1}$ )	0.186
Temkin $q_e = \frac{RT}{b_T} \ln (A_T C_e)$	$b_T$ ( $\text{J mol}^{-1}$ )	125.6
	$R^2$	0.945

**Table 4.** Isotherm constants and correlation coefficients obtained for the removal of  $\text{Cd}^{2+}$  ions by CuS nanorods.

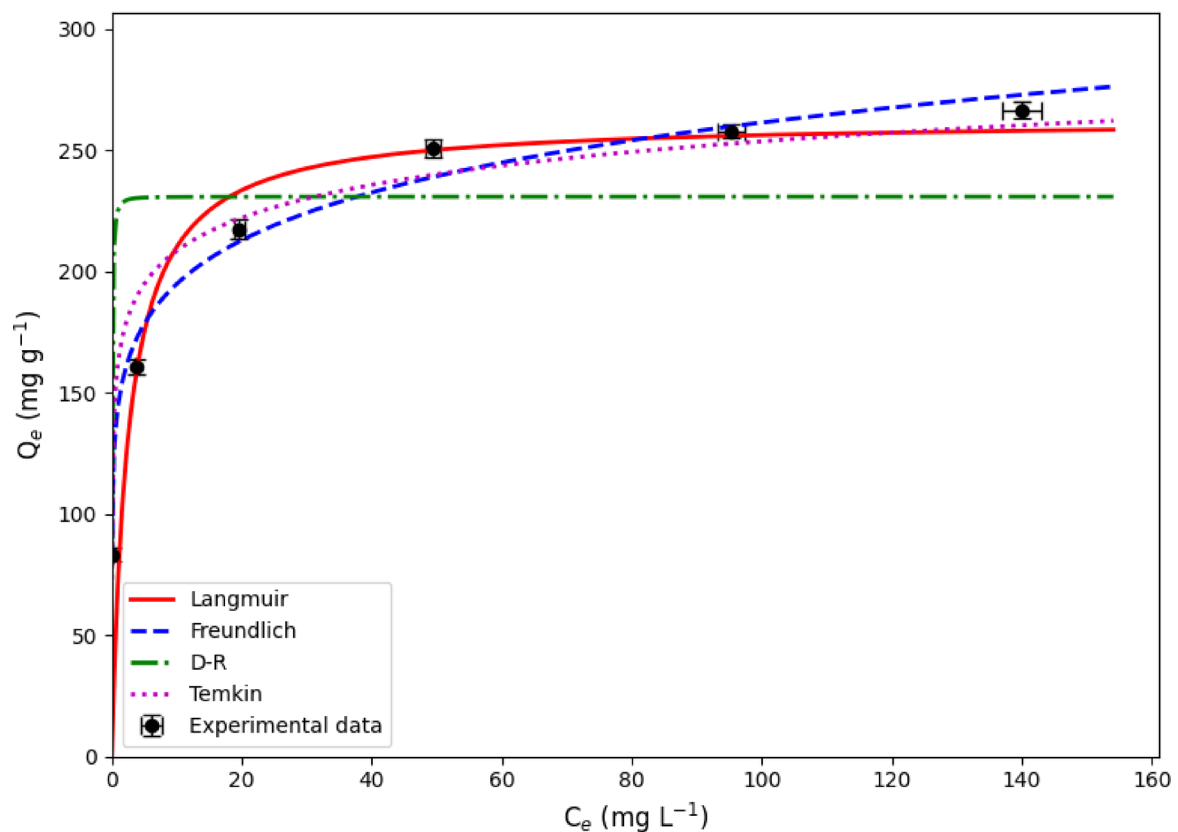


**Fig. 8.** Adsorption isotherm plots for the removal of  $\text{Cd}^{2+}$  ions by CuS nanorods (pH-6 contact time: 90 min and CuS nanorods dose  $1.5 \text{ g L}^{-1}$ ).

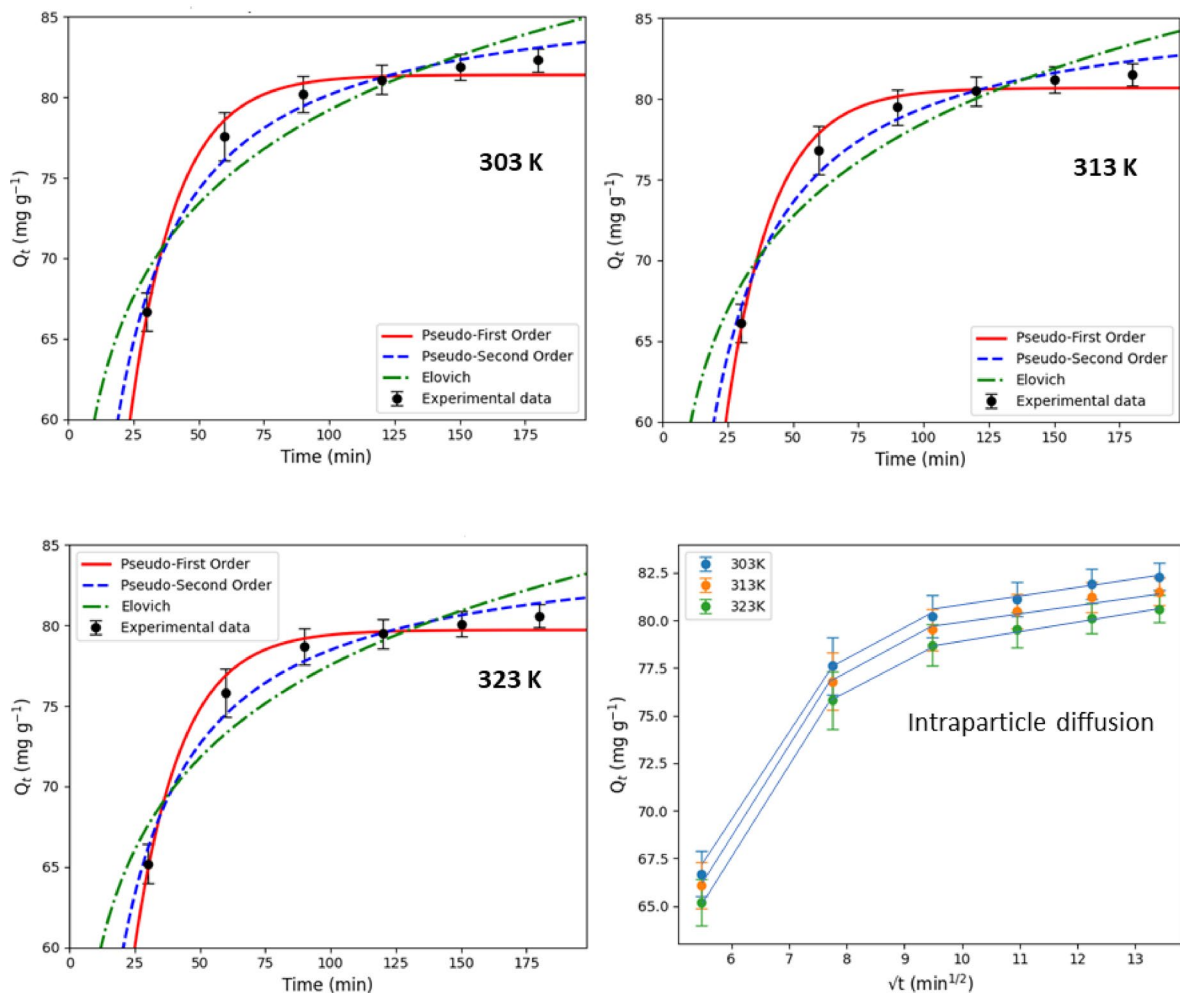
Isotherm	MSE	RMSE	MAE	$\chi^2$	$R^2$
Langmuir	45.21	6.72	5.89	2.14	0.991
Freundlich	118.6	10.89	9.12	5.63	0.963
D-R	78.95	8.89	7.45	3.74	0.978
Temkin	162.84	12.76	10.53	7.71	0.945

**Table 5.** Error metrics calculated for the isotherm models used for the removal of  $\text{Cd}^{2+}$  ions by CuS nanorods.

Model	Parameters	Values		
		303 K	313 K	323 K
Pseudo first order	$k_1 (\text{min}^{-1})$	0.0314	0.0387	0.0452
	$q_e (\text{mg g}^{-1})$	83.12	82.45	81.68
	$R^2$	0.984	0.981	0.978
Pseudo second order	$k_2 (\text{min}^{-1})$	0.0005	0.0006	0.0008
	$q_e (\text{mg g}^{-1})$	84.25	83.61	82.93
	$R^2$	0.998	0.997	0.996
Intraparticle diffusion	$k_{it} (\text{mg gmin}^{0.5})$	5.12	5.87	6.45
	$C (\text{mg g}^{-1})$	45.21	43.78	42.15
	$R^2$	0.962	0.958	0.953
Elovich	$\alpha$	0.063	0.051	0.042
	$\beta$	0.072	0.079	0.085
	$R^2$	0.972	0.968	0.963

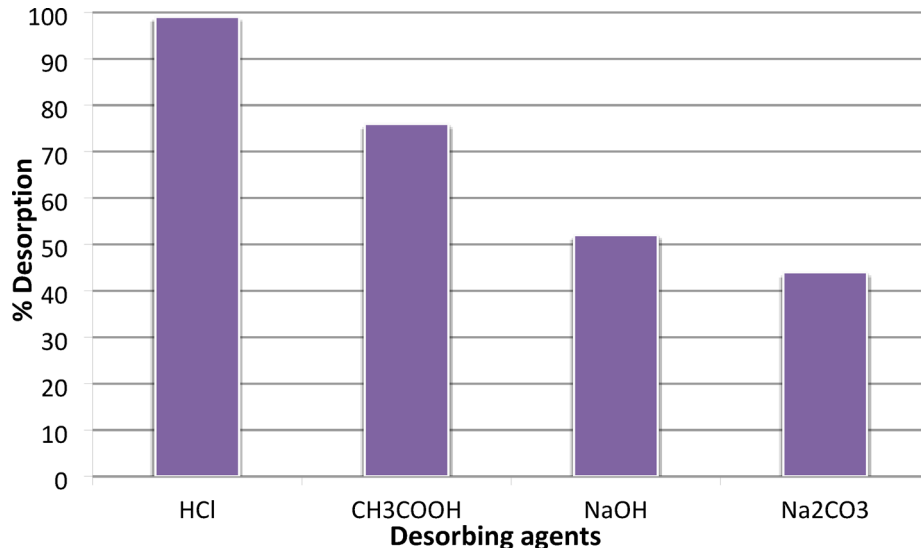
**Table 6.** Kinetic parameters calculated for the removal of  $\text{Cd}^{2+}$  ions by CuS nanorods.

Model	Temp	MSE	RMSE	MAE	$\chi^2$	$R^2$
Pseudo first order	303 K	12.34	3.51	2.89	1.87	0.984
	313 K	14.21	3.77	3.12	2.15	0.981
	323 K	16.05	4.01	3.45	2.43	0.978
Pseudo second order	303 K	1.02	1.01	0.85	0.15	0.998
	313 K	1.35	1.16	0.97	0.21	0.997
	323 K	1.78	1.33	1.12	0.28	0.996
Intraparticle diffusion	303 K	18.92	4.35	3.78	3.01	0.962
	313 K	20.45	4.52	4.05	3.32	0.958
	323 K	22.17	4.71	4.31	3.68	0.953
Elovich	303 K	15.23	0.90	3.45	2.42	0.972
	313 K	17.45	4.19	3.78	2.81	0.968
	323 K	19.87	4.46	4.12	3.19	0.963

**Table 7.** Error metrics calculated for the kinetic models used for the removal of  $\text{Cd}^{2+}$  ions by CuS nanorods.**Fig. 9.** Kinetic plots for the removal of  $\text{Cd}^{2+}$  ions by CuS nanorods (pH 6, initial concentration  $50 \text{ mg L}^{-1}$  and CuS nanorods dose  $1.5 \text{ g L}^{-1}$ ).

interesting results with applicability of Pseudo first and second order kinetic models to the kinetic data<sup>44</sup>. The correlation coefficients and  $q_e$  values obtained for both the models are close to each other with well agreement to the experimental results at all temperatures studied. The  $q_e$  values for the both the kinetic models were found to decrease with increase in temperature suggesting that the rate of adsorption is influenced by the temperature. Further the decreasing  $\alpha$  values observed from Elovich equation suggests that the adsorption rate is high at lower

Temp (K)	qe (mg g <sup>-1</sup> )	ln k <sub>e</sub>	ΔG° (kJ mol <sup>-1</sup> )	ΔH° (kJ mol <sup>-1</sup> )	ΔS° (kJ mol K <sup>-1</sup> )
303	84.25	0.522	- 1.34	- 2.15	- 0.0029
313	83.61	0.514	- 1.30		
323	82.93	0.506	- 1.26		

**Table 8.** Thermodynamic parameters for the removal of Cd<sup>2+</sup> ions by CuS nanorods.**Fig. 10.** Regeneration and reusability of CuS nanorods synthesised using jamun seeds aqueous extract (Time 90 min and Temperature 303 K).

temperatures for Cd<sup>2+</sup> ions by CuS nanorods. To ascertain the rate governing step in this study, efforts were made to calculate the activation energy (E<sub>a</sub>) from Arrhenius equation. The activation energy was calculated to be 24.73 kJ mol<sup>-1</sup> which suggest the physical adsorption with some weak chemical interactions for the removal of Cd<sup>2+</sup> ions by CuS nanorods<sup>45</sup>. The intraparticle diffusion study revealed multi step plot suggesting that pore diffusion is not the sole rate limiting step. Further error metrics were performed for each kinetic model at all temperatures and the results are summarized Table-7 and it is noticed that pseudo second order kinetic model has lowest errors across all temperatures. It is also noticed that errors increase with temperature but in the case of pseudo second order it is consistent. These results suggest the better applicability of the pseudo second order kinetic model for the removal of Cd<sup>2+</sup> ions by CuS nanorods.

### Thermodynamics of adsorption

Thermodynamic investigations revealed pivotal information on the nature of the adsorption of Cd<sup>2+</sup> ions removal by CuS nanorods and the results are presented in Table 8. It is noticeable that the loading capacity decreases with rise in temperature suggesting that the higher temperature Cd<sup>2+</sup> ions adsorption onto CuS nanorods are not favourable as noticed in Elovich model. The free energy at studied temperature are found to be negative suggesting the spontaneous nature of removal of Cd<sup>2+</sup> ions by CuS nanorods and the negative values decrease with rise in temperature indicates higher temperatures are unfavourable. The enthalpy value was found to be negative indicating the exothermic nature of the process and negative entropy value indicates the slight decrease in randomness at surface<sup>46</sup>.

### Regeneration and reusability studies

The CuS nanorods ability to regenerate and reuse for multiple cycles in the adsorption of Cd<sup>2+</sup> ions were evaluated by desorption studies and results are presented in Fig. 10. Various desorbing agents such as 0.01 M HCl, 0.01 M CH<sub>3</sub>COOH, 0.01 M NaOH and 0.01 M Na<sub>2</sub>CO<sub>3</sub> were testing for their ability to regenerate the CuS nanorods and it is noticed that 0.01 M HCl exhibited highest desorption percentage of 99% compared to other three agents selected in this study. The superior efficiency of HCl is due to immediate dissociation of H<sup>+</sup> ions and that could replace the Cd<sup>2+</sup> ions from the active sites of the CuS nanorods. The regenerated CuS nanorods were successfully reused in the adsorption of CuS nanorods for five cycles without any loss in its adsorption capacity. The adsorption capacities for all the five cycles were found to be 84 ± 0.5 mg g<sup>-1</sup> at optimal conditions. These results prove the capability of the CuS nanorods to reuse multiple cycles without any loss of its capacity towards adsorption of Cd<sup>2+</sup> ions.

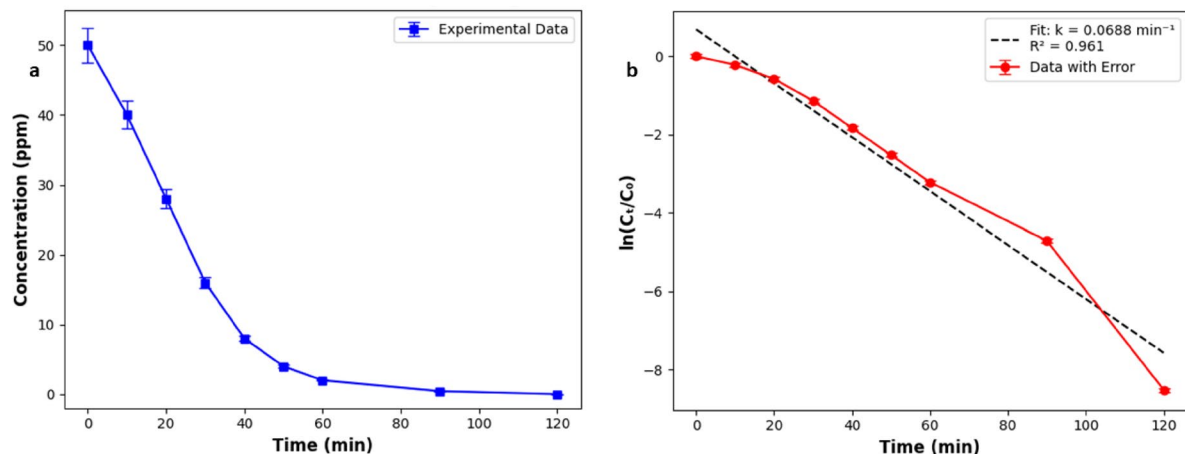


**Fig. 11.** Plots of degradation with respect to (a) time and (b) first order kinetics for MO by CuS nanorods (pH 3, initial concentration  $50 \text{ mg L}^{-1}$  and CuS nanorods dose  $1.5 \text{ g L}^{-1}$ ).

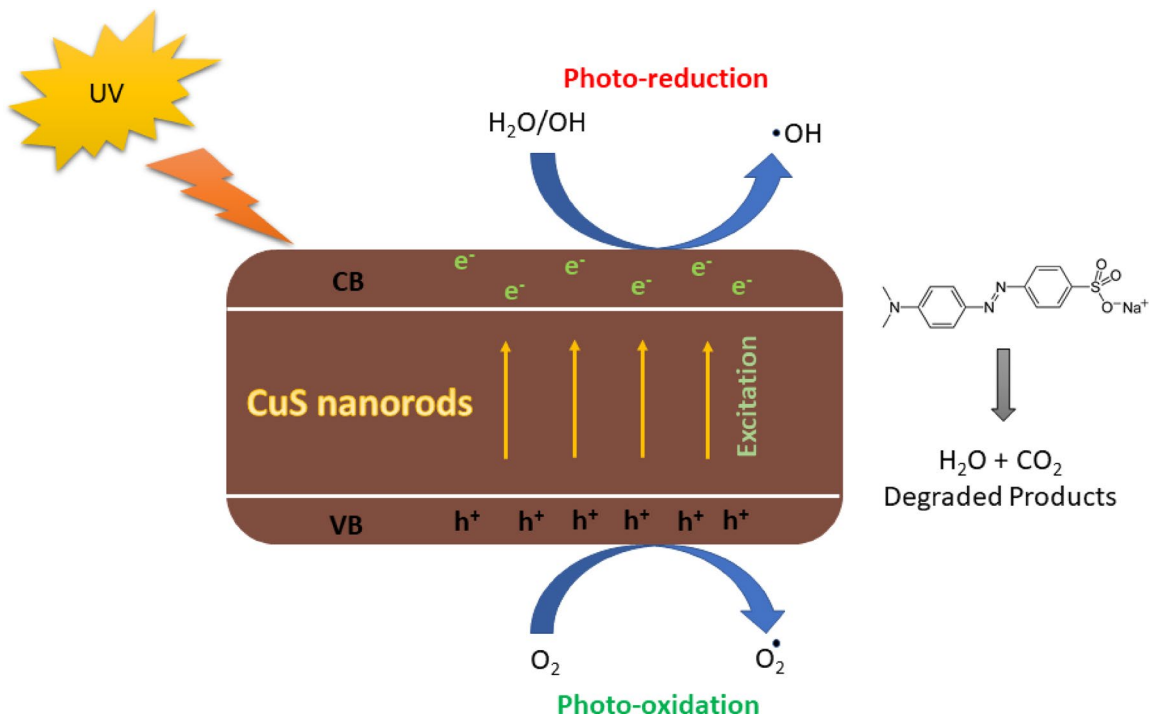


**Fig. 12.** Mechanism of photocatalytic degradation of MO by CuS nanorods.

### Photocatalytic degradation of Methyl Orange

The photocatalytic efficiency of the CuS nanorods were evaluated towards photodegradation of Methyl orange (MO) dye and the results are presented in Fig. 11. A complete photodegradation of MO ( $50 \text{ mg L}^{-1}$ ) was achieved within 120 min of time when it was exposed to CuS nanorods ( $1.5 \text{ g L}^{-1}$ ) in presence of UV light at pH 3. The rapid efficiency exhibited by the CuS nanorods is due to their rod shaped providing ample sites for the quick adsorption of MO onto their surface. The narrow band gap of  $1.9 \text{ eV}$  calculated for CuS nanorods in this study excites electrons to conduction band providing the holes in the valence band thus producing radicals and these free radicals instantly attack the MO to degrade into  $CO_2$  and  $H_2O$  molecules Fig. 12. The high photodegradation efficiency at pH 3 is attributed to a synergistic mechanism. The acidic environment induces a positive surface charge on the CuS nanorods (pH<sub>PZC</sub> of 3.7), facilitating strong electrostatic attraction and adsorption of the anionic Methyl Orange dye. Concurrently, the production of reactive oxygen species (ROS), particularly hydroxyl radicals ( $\cdot OH$ ) and superoxide radicals ( $\cdot O_2$ ), under light irradiation is highly favourable at this pH<sup>47,48</sup>. The high local concentration of pre-adsorbed dye molecules on the catalyst surface ensures their immediate and efficient attack by the photogenerated ROS, resulting in rapid and efficient degradation<sup>49</sup>. In

Species	Concentration	Zone of inhibition
<i>E. coli</i>	25 $\mu$ L	25 mm
<i>S. aureus</i>	25 $\mu$ L	26 mm
Streptomycin disc	–	25 mm

**Table 9.** ZOI exhibited by the CuS nanorods towards gram positive and negative microbes.

addition, the efficiency is due to broader wavelength of absorption of energy in visible and NIR region that enhances the photocatalytic activity of CuS nanorods. The degradation data was analysed with pseudo first order kinetics and it obtained a liner fit with a  $R^2$  of 0.961 suggesting the better fit of the model. The rate constant was calculated to be  $k_{obs} = 0.0688 \text{ min}^{-1}$  with a half-life of 10.1 min. These results suggest the potential of CuS nanorods in photocatalytic degradation of Methyl orange with high efficiency.

### Antimicrobial activity

The CuS nanorods were assessed for their antimicrobial activity against *E. coli* and *S. aureus* and the resulting ZOI are presented in Table 9. The CuS nanorods exhibited superior antimicrobial activity against the tested pathogens with a ZOI of 25 and 26 mm respectively for *E. coli* and *S. aureus*. The ZOI exhibited by CuS nanorods at 25  $\mu$ L were equal to that of standard streptomycin disc (25 mm). The higher inhibition exhibited by the CuS nanorods are due to their small size with rod shape and potential to absorb light in visible range<sup>50</sup>. The mechanism of CuS nanorods for the superior activity can be attributed to multiple routes that could have synergistically catered for the overall activity. Firstly, the CuS nanorods are capable of releasing  $\text{Cu}^{2+}$  ions that can bind to the thiol groups of the proteins and thus resulting in the disruptions of the microbial cell wall. Secondly the CuS nanorods are capable of generating reactive oxygen species (ROS) that damage the DNA and lipids of the microbes. Lastly, the physical shape of the nanorods with sharp edges can damage the cells of microbes allowing the Cu ions and ROS to enter and damage the lipids and proteins. The above mechanistic paths are possible in absence of light and CuS nanorods are capable of absorbing NIR light and photothermally kill the microbes which can synergistically enhance the overall activity of the CuS nanorods<sup>50</sup>. The results highlight the potential of CuS nanorods synthesised in this study as an antimicrobial agent. Although the results successfully identified the microbial activity by well-diffusion method, for quantitative analysis, MIC determination is required to understand the potential of the CuS nanorods.

### Conclusion

This study successfully demonstrated the green synthesis of CuS nanorods using jamun seeds aqueous extract. The CuS nanorods formations were evidenced from analytical techniques such as UV-Vis, SEM and TEM. The CuS nanorods were explored in the adsorption of  $\text{Cd}^{2+}$  ions and independent variables were optimised using BBD of RSM. The ANOVA results highlight the reliability of the design with significant values and adequate precision was found to be 72.42 with a standard deviation of 1.37. Though all four isotherms used in this study found to have good correlation coefficients, error analysis highlighted the applicability of the Langmuir model followed by D-R isotherm. The mean potential energy ( $E_s$ ) calculated from D-R isotherm highlights the ion-exchange mechanism governing the adsorption of  $\text{Cd}^{2+}$  ions by CuS nanorods. Pseudo second order kinetic model is found to be the best applicable model based on the error analysis compared to other kinetic models. Activation energy of 24.73  $\text{kJ mol}^{-1}$  suggests the physical adsorption of  $\text{Cd}^{2+}$  ions by CuS nanorods with multi step process evidenced from intraparticle diffusion. The rate of reaction and loading capacity decreases with rise in temperature and found to be spontaneous and favourable at low temperatures. The MO dye was 100% degraded within 120 min in presence of UV source by CuS nanorods highlighting the ability of the CuS nanorods in degrading complex and recalcitrant molecules. The CuS nanorods exhibited excellent antimicrobial activity against two pathogens such as *E. coli* and *S. aureus* and a synergy of mechanism was involved in the antimicrobial activity. The results of this study establish the multifunctional ability of the CuS nanorods synthesised via green route using jamun seeds extract and highlights a stop sustainable material for multi applications in clean water management.

### Data availability

All the data are available within the manuscript and any additional data are available from corresponding author on reasonable request.

Received: 11 July 2025; Accepted: 22 September 2025

Published online: 27 October 2025

### References

- Sharma, K., Rajan, S. & Nayak, S. K. Water pollution: primary sources and associated human health hazards with special emphasis on rural areas. In *Water Resources Management for Rural Development* 3–14 (Elsevier, 2024).
- World Health Organization. *Drinking-Water*. <https://www.who.int/news-room/fact-sheets/detail/drinking-water> (2024).
- Crini, G. & Lichfouse, E. Advantages and disadvantages of techniques used for wastewater treatment. *Environ. Chem. Lett.* **17**, 145–155. <https://doi.org/10.1007/s10311-018-0785-9> (2019).
- Sharma, N., Singh, A. & Batra, N. Modern and emerging methods of wastewater treatment. *Ecol. Wisdom Inspired Restor. Eng.* 223–247. [https://doi.org/10.1007/978-981-13-0149-0\\_13](https://doi.org/10.1007/978-981-13-0149-0_13) (2019).

5. Sukmana, H., Bellahsen, N., Pantoja, F. & Hodur, C. Adsorption and coagulation in wastewater treatment—Review. *Prog Agric. Eng. Sci.* **17** (1), 49–68. <https://doi.org/10.1556/446.2021.00029> (2021).
6. Tran, H. N. Adsorption technology for water and wastewater treatments. *Water* **15** (15), 2857. <https://doi.org/10.3390/w15152857> (2023).
7. Epelle, E. I., Okoye, P. U., Roddy, S., Gunes, B. & Okolie, J. A. Advances in the applications of nanomaterials for wastewater treatment. *Environments* **9** (11), 141. <https://doi.org/10.3390/environments9110141> (2022).
8. Zhang, Y. et al. Nanomaterials-enabled water and wastewater treatment. *NanoImpact* **3**, 22–39. <https://doi.org/10.1016/j.impact.2016.09.004> (2016).
9. Singh, P. et al. Nanomaterials photocatalytic activities for waste water treatment: a review. *Environ. Sci. Pollut. Res.* **29** (46), 69294–69326. <https://doi.org/10.1007/s11356-022-22550-7> (2022).
10. Mishra, S. & Sundaram, B. A review of the photocatalysis process used for wastewater treatment. *Mater. Today Proc.* **102**, 393–409. <https://doi.org/10.1016/j.matpr.2023.07.147> (2024).
11. Alqarni, L. S., Alghamdi, M. D., Alshahrani, A. A. & Nassar, A. M. Green nanotechnology: recent research on bioresource-based nanoparticle synthesis and applications. *J. Chem.* **2022** (1), 4030999. <https://doi.org/10.1155/2022/4030999> (2022).
12. Rambabu, K., Bharath, G., Banat, F. & Show, P. L. Green synthesis of zinc oxide nanoparticles using Phoenix dactylifera waste as bioreductant for effective dye degradation and antibacterial performance in wastewater treatment. *J. Hazard. Mater.* **402**, 123560. <https://doi.org/10.1016/j.jhazmat.2020.123560> (2021).
13. Demarema, S., Nasr, M., Ookawara, S. & Abdelhaleem, A. New insights into green synthesis of metal oxide based photocatalysts for photodegradation of organic pollutants: A bibliometric analysis and techno-economic evaluation. *J. Clean. Prod.* **142**679. <https://doi.org/10.1016/j.jclepro.2024.142679> (2024).
14. Eddy, D. R. et al. A review of recent developments in green synthesis of TiO<sub>2</sub> nanoparticles using plant extract: Synthesis, characterization and photocatalytic activity. *Inorg. Chem. Commun.* **112531**. <https://doi.org/10.1016/j.inoche.2024.112531> (2024).
15. Gemachu, L. Y. & Birhanu, L. A. Green synthesis of ZnO, CuO and NiO nanoparticles using Neem leaf extract and comparing their photocatalytic activity under solar irradiation. *Green. Chem. Lett. Rev.* **17** (1), 2293841. <https://doi.org/10.1080/17518253.2023.2293841> (2024).
16. Abegunde, S. M., Adebayo, M. A. & Olasehinde, E. F. Green synthesis of ZnO nanoparticles and its application for Methyl green dye adsorption. *Green. Energy Resour.* **2** (2), 100073. <https://doi.org/10.1016/j.gerr.2024.100073> (2024).
17. Abed, A. Q., Al Hindawi, A. M. & Alesary, H. F. Green synthesis of zinc sulfide nanoparticles for the removal of methylene blue dye from aqueous solution. *Nano World J.* **8**, 79–84. <https://doi.org/10.17756/nwj.2022-103> (2022).
18. Elakkiya, G. T., Sundararajan, G., LakshmiPathy, R., Anitha, P. & Muruganantham, N. Prolific application of green synthesised cds nanoparticles for the sequestration of cationic dyes from aqueous solution. *Bull. Chem. Soc. Ethiop.* **38** (3), 631–645. <https://doi.org/10.4314/bcse.v38i3.7> (2024).
19. Alangari, A. et al. Green synthesis of copper oxide nanoparticles using genus Inula and evaluation of biological therapeutics and environmental applications. *Nanotechnol Rev.* **13** (1), 2024009. <https://doi.org/10.1515/ntrev-2024-0039> (2024).
20. Borah, D. et al. Composition controllable alga-mediated green synthesis of covellite CuS nanostructure: an efficient photocatalyst for degradation of toxic dye. *Inorg. Chem. Commun.* **142**, 109608. <https://doi.org/10.1016/j.inoche.2022.109608> (2022).
21. Ayodhya, D. et al. Photocatalytic degradation of dye pollutants under solar, visible and UV lights using green synthesised CuS nanoparticles. *J. Exp. Nanosci.* **11** (6), 418–432. <https://doi.org/10.1080/17458080.2015.1070312> (2016).
22. Bharti, S. Recent advances in heavy metal removal from wastewater using nanomaterials and cloud point extraction: A comprehensive review. *Int. J. Environ. Sci. Technol.* **22** (6), 5057–5084. <https://doi.org/10.1007/s13762-024-06068-8> (2025).
23. Kishor, R. et al. Degradation mechanism and toxicity reduction of Methyl orange dye by a newly isolated bacterium *Pseudomonas aeruginosa* MZ520730. *J. Water Process. Eng.* **43**, 102300. <https://doi.org/10.1016/j.jwpe.2021.102300> (2021).
24. Akansha, K., Chakraborty, D. & Sachan, S. G. Decolorization and degradation of Methyl orange by *Bacillus stratosphericus* SCA1007. *Biocatal. Agric. Biotechnol.* **18**, 101044. <https://doi.org/10.1016/j.biocab.2019.101044> (2019).
25. Golabiazzar, R. et al. Green biosynthesis of cds NPs and cds/Fe3O4 NCS by Hawthorn plant extract for photodegradation of Methyl orange dye and antibacterial applications. *J. Clust Sci.* **33**, 1223–1238. <https://doi.org/10.1007/s10876-021-02054-z> (2022).
26. Rezaei, M., Nezamzadeh-Ejhieh, A. & Massah, A. R. A comprehensive review on the boosted effects of anion vacancy in the heterogeneous photocatalytic degradation, part II: focus on oxygen vacancy. *ACS Omega.* **9** (6), 6093–6127. <https://doi.org/10.1021/acsomega.3c07560> (2024).
27. Alghamdi, S. Q. et al. High antiparasitic and antimicrobial performance of biosynthesized NiO nanoparticles via wasted Olive leaf extract. *Int. J. Nanomed.* **19**, 1469–1485. <https://doi.org/10.2147/IJN.S443965> (2024).
28. Mondal, S. K., Chakraborty, S., Manna, S. & Mandal, S. M. Antimicrobial nanoparticles: current landscape and future challenges. *RSC Pharm.* **1** (3), 388–402. <https://doi.org/10.1039/D4PM00032C> (2024).
29. She, P. et al. Photocatalytic antibacterial agents based on inorganic semiconductor nanomaterials: a review. *Nanoscale* **16** (10), 4961–4973. <https://doi.org/10.1039/D3NR06531F> (2024).
30. Yang, J. et al. Biosynthesis of CuS nanozymes for synergistic antibacterial applications: biosynthetic parameters optimization and antimicrobial mechanism Elucidation. *J. Colloid Interface Sci.* **138604**. <https://doi.org/10.1016/j.jcis.2025.138604> (2025).
31. Ayyanar, M. & Subash-Babu, P. *Syzygium cumini* (L.) skeels: A review of its phytochemical constituents and traditional uses. *Asian Pac. J. Trop. Biomed.* **2** (3), 240–246. [https://doi.org/10.1016/S2221-1691\(12\)60050-1](https://doi.org/10.1016/S2221-1691(12)60050-1) (2012).
32. Wang, W. & Ao, L. Synthesis and characterization of crystalline CuS nanorods prepared via a room temperature one-step, solid-state route. *Mater. Chem. Phys.* **109** (1), 77–81. <https://doi.org/10.1016/j.matchemphys.2007.10.035> (2008).
33. Roy, P. & Srivastava, S. K. Low-temperature synthesis of CuS nanorods by simple wet chemical method. *Mater. Lett.* **61** (8–9), 1693–1697. <https://doi.org/10.1016/j.matlet.2006.07.101> (2007).
34. Shahi, N., Rahmati, A., Khanzadeh, M. & Near IR light sensitization modulated to self-assembled CuO–CuxS nanorods thin films. *Opt. Mater.* **148**, 114800. <https://doi.org/10.1016/j.optmat.2023.114800> (2024).
35. Fatolahi, L. Preparation of CuS/CuO on decoration graphene oxide nanocomposites for the photocatalytic degradation of gaseous phase based on UV light irradiation, and evaluation of toxicology on bacterial cells. *J. Inorg. Organomet. Polym. Mater.* **34** (5), 2030–2041. <https://doi.org/10.1007/s10904-023-02945-w> (2024).
36. Mishra, S. R., Panigrahi, B., Gadore, V., Sarkar, N. & Ahmaruzzaman, M. Enhanced photocatalytic performance of CuS/O, N-CNT composite for solar-driven organic contaminant degradation. *Sci. Rep.* **14** (1), 18022. <https://doi.org/10.1038/s41598-024-68770-4> (2024).
37. Parveen, S. T. & Riazunnisa, K. Phytofabrication of copper nanoparticles using momordica cymbalaria fruit extract and their antibacterial, antioxidant and anti-inflammatory properties. *Hybrid. Adv.* **9**, 100421. <https://doi.org/10.1016/j.hybadv.2025.100421> (2025).
38. Barnwal, K. S., Gupta, Y. & Jaggi, N. Green synthesis of copper sulphide nanoparticles using extracts of *Syzygium cumini*, *Azadirachta indica*, and *Cascabela Thevetia*. *J. Electron. Mater.* **53** (11), 6613–6623. <https://doi.org/10.1007/s11664-024-11387-0> (2024).
39. Nath, S. K. & Kalita, P. K. Temperature dependent structural, optical and electrical properties of CuS nanorods in Aloe Vera matrix. *Nano-Struct Nano-Objects.* **25**, 100651. <https://doi.org/10.1016/j.nanoso.2020.100651> (2021).
40. Alqahtani, M. S. et al. An eco-friendly synthesis of ZnO nanoparticles with Jamun seed extract and their multi-applications. *Rev. Adv. Mater. Sci.* **64** (1), 20250134. <https://doi.org/10.1515/rams-2025-0134> (2025).

41. Alprol, A. E. et al. Chitosan/ferrous oxide nanocomposite for the sunlight-driven photocatalytic degradation of organic Azo dye in aqueous solutions and aquaculture effluents wastewater. *Sci. Rep.* **15** (1), 23289. <https://doi.org/10.1038/s41598-025-04207-w> (2025).
42. Han, D., Villanueva-Tagle, M. E., Peña-Icart, M., López-Mesas, M. & Valiente, M. Trace cisplatin adsorption by thiol-functionalized sponge (TFS) and Sn/SnO<sub>2</sub>-coated TFS: adsorption study and mechanism investigation. *J. Hazard. Mater.* **471**, 134442. <https://doi.org/10.1016/j.jhazmat.2024.134442> (2024).
43. Kul, A. R. & Aldemir, A. An investigation of aniline removal performance by the activated carbon prepared from biomass conversion: adsorption results of isotherm, kinetic and thermodynamic studies. *Biomass Convers. Biorefinery.* **1**, 1–16. <https://doi.org/10.1007/s13399-024-06433-0> (2024).
44. Guerrero-Fajardo, C. A., Giraldo, L. & Moreno-Pirajan, J. C. Isotherm, thermodynamic, and kinetic studies of dye adsorption on graphene oxides with varying oxidation degrees. *Results Eng.* **26**, 104558. <https://doi.org/10.1016/j.rineng.2025.104558> (2025).
45. Wang, H., Wang, S., Wang, S., Fu, L. & Zhang, L. Efficient metal-organic framework adsorbents for removal of harmful heavy metal Pb (II) from solution: activation energy and interaction mechanism. *J. Environ. Chem. Eng.* **11** (2), 109335. <https://doi.org/10.1016/j.jece.2023.109335> (2023).
46. Dai, L. et al. Enhanced removal of Cd<sup>2+</sup> by nano zero-valent iron modified attapulgite from aqueous solution: optimal design, characterization and adsorption mechanism. *J. Environ. Chem. Eng.* **10** (3), 107719. <https://doi.org/10.1016/j.jece.2022.107719> (2022).
47. Alqarni, L. S. et al. Photocatalytic degradation of rhodamine-B and water densification via eco-friendly synthesized Cr<sub>2</sub>O<sub>3</sub> and Ag@Cr<sub>2</sub>O<sub>3</sub> using Garlic Peel aqueous extract. *Nanomaterials* **14** (3), 289. <https://doi.org/10.3390/nano14030289> (2024).
48. Lopes, I. S. et al. Green synthesis of antimicrobial silver-copper nanoparticles using banana and pineapple Peel extracts: A sustainable approach for biomaterial sterilization. *Mater. Chem. Phys.* **333**, 130364. <https://doi.org/10.1016/j.matchemphys.2025.130364> (2025).
49. Mishra, N., Gahlaut, U. P. S. & Goswami, Y. C. Eco-friendly synthesis of copper sulphide nanoparticles using rice starch water and their photocatalytic application for congo red dye degradation. *Next Nanotechnol.* **8**, 100200. <https://doi.org/10.1016/j.nxnano.2025.100200> (2025).
50. Barnwal, K. S., Gupta, Y. & Jaggi, N. Plants-extracts mediated CuS nanoparticles: an effective antibacterial agent. *Surf. Interfaces.* **55**, 105326. <https://doi.org/10.1016/j.surfin.2024.105326> (2024).

## Acknowledgements

The authors extend their appreciation to University Higher Education Fund for funding this research work under Research Support Program for Central Labs at King Khalid University through the project number CL/CO/A/6.

## Author contributions

RL: Investigation, Formal analysis, Manuscript writing, Conceptualization; SR: Investigation, Manuscript writing; SVP: Investigation, Data analysis; MA: Conceptualization, Manuscript review, Funding; NA: Conceptualization, Manuscript reviewing and editing.

## Funding

The authors extend their appreciation to University Higher Education Fund for funding this research work under Research Support Program for Central Labs at King Khalid University through the project number CL/CO/A/6.

## Declarations

### Competing interests

The authors declare no competing interests.

### Additional information

**Supplementary Information** The online version contains supplementary material available at <https://doi.org/10.1038/s41598-025-21619-w>.

**Correspondence** and requests for materials should be addressed to N.A.

**Reprints and permissions information** is available at [www.nature.com/reprints](http://www.nature.com/reprints).

**Publisher's note** Springer Nature remains neutral with regard to jurisdictional claims in published maps and institutional affiliations.

**Open Access** This article is licensed under a Creative Commons Attribution-NonCommercial-NoDerivatives 4.0 International License, which permits any non-commercial use, sharing, distribution and reproduction in any medium or format, as long as you give appropriate credit to the original author(s) and the source, provide a link to the Creative Commons licence, and indicate if you modified the licensed material. You do not have permission under this licence to share adapted material derived from this article or parts of it. The images or other third party material in this article are included in the article's Creative Commons licence, unless indicated otherwise in a credit line to the material. If material is not included in the article's Creative Commons licence and your intended use is not permitted by statutory regulation or exceeds the permitted use, you will need to obtain permission directly from the copyright holder. To view a copy of this licence, visit <http://creativecommons.org/licenses/by-nc-nd/4.0/>.

© The Author(s) 2025